Supplemental Materials for

Global loss of cellular m^{6}A RNA methylation following infection with different SARS-CoV-2 variants

Vaid, Mendez, *et al*

Department of Clinical Chemistry and Transfusion Medicine, Sahlgrenska University Hospital,

Gothenburg University, Gothenburg, Sweden.

Contents

Other Supplementary Materials for this manuscript

Supplemental Data S1: Differentially expressed genes following SARS-CoV-2 infection in Vero and HBE cells

Supplemental Data S2: Enrichment analysis of differentially expressed genes following SARS-CoV-2 infection in Vero and HBE cells.

Supplemental Data S3: m^{6}A peaks in the SARS-CoV-2 viral genome and in the host genomes of Noninfected and SARS-CoV-2 infected Vero, HBE, and HNE.

Supplemental Data S4: Genes with differential exon usage (DEU) in SARS-CoV-2 infected Vero cells.

Supplemental Figure S1

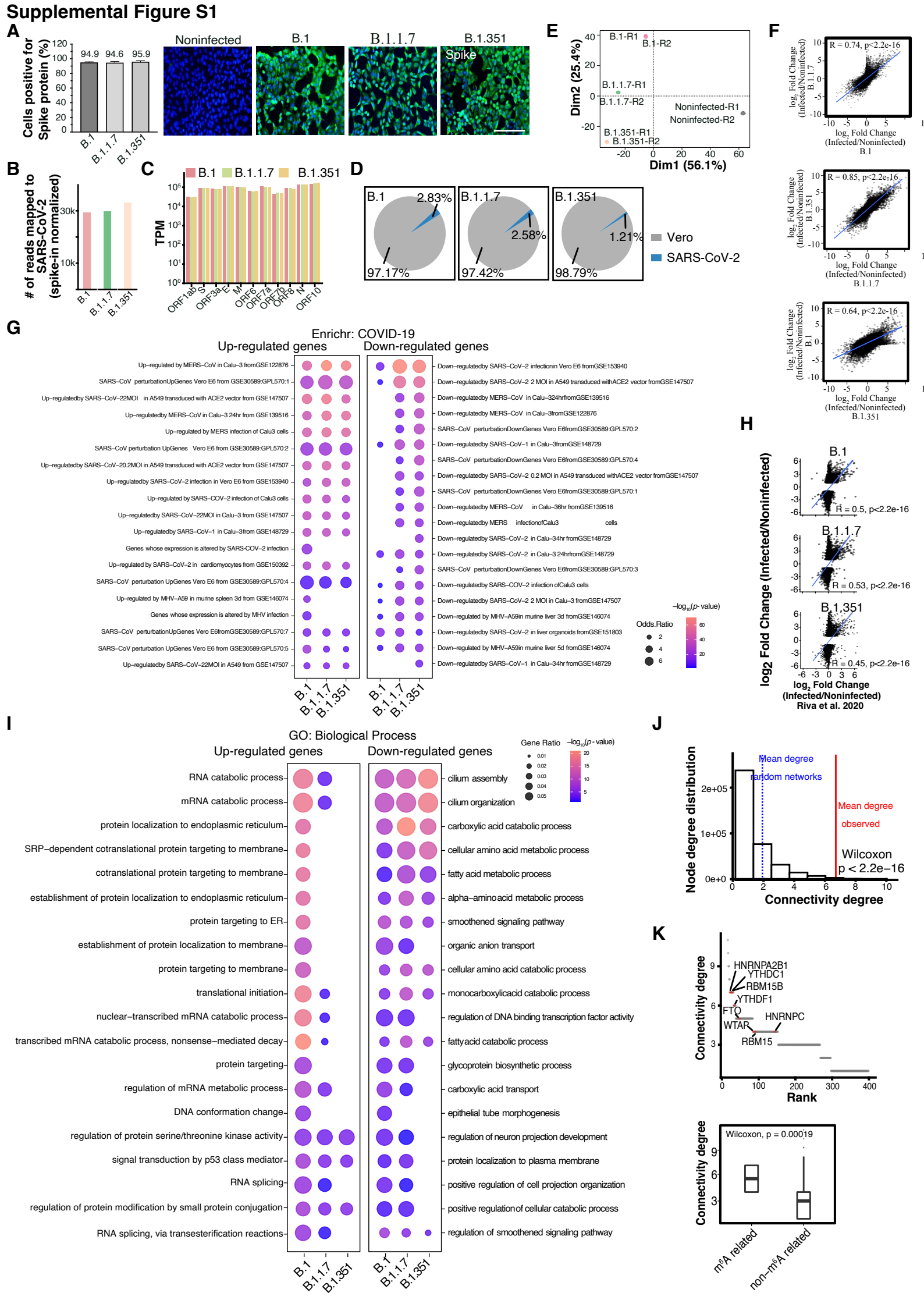

Supplemental_Figure_S1 (A) SARS-CoV-2 Spike protein staining summarized as bar plots with mean ± SD shown (left panel; n=2) and corresponding representative images of Spike staining (right panel) in Vero cells 48 h post-infection with three different SARS-CoV-2 variants as indicated. The scale bar is 200 μm. (B) Bar plots showing spike-in normalized reads mapped to the SARS-CoV-2 genome in Vero cells infected with different variants of SARS- CoV-2. (C) The $\log_{10}$ transcripts per million (TPM) values for SARS-CoV-2 genes in B.1, B.1.1.7, and B.1.351 infected cells. Data shown as the mean of two replicates. (D) Pie chart showing the percentage of reads mapping to host (Vero) and viral (SARS-CoV-2) genomes. (E) Principal-component analysis (PCA) of global expression patterns of SARS-CoV-2 infected (variants as specified) and noninfected Vero cells. Replicates are labelled with R1 and R2 suffixes. (F) Scatter plots showing correlation between $\log_2$ fold changes in gene expression after infection with different SARS-CoV-2 variants in Vero cells. Statistics: Pearson's correlation test. The blue line shows the linear regression with 95% confidence interval. (G) Top enriched terms associated with up-regulated and down-regulated genes after SARS-CoV-2 infection, based on publicly available COVID-19 related gene sets. Data were obtained from the Enrichr database. (H) Scatter plots of differentially expressed genes depicting the correlation between the $\log_2$ fold changes in gene expression after B.1, B.1.1.7, and B.1.351 infection and the $\log_2$ fold changes reported in publicly available data of SARS- CoV-2 infected Vero cells 24-hour post infection (Riva et al., 2020). The blue line depicts the linear regression line with 95% confidence interval. Statistics: Pearson's correlation test. (I) Top GO biological process terms associated with up-regulated and down-regulated genes after infection of Vero cells with the B.1, B.1.1.7, and B.1.351 strains. The size of the dots represents the enrichment of genes for a given GO term; the dots are colored according to their significance in $\log_{10}$ *p*-value. (J) Node connectivity degree distribution of 1000 randomly generated networks of the same size. The mean connectivity of random networks (blue dotted line) was compared to the observed mean connectivity degree of the network obtained after ClueGO analysis for RNA catabolism-associated genes (red line). Statistical significance was calculated using the Wilcoxon signed rank test. (K, top panel) Ranking of nodes according to their connectivity degree, with m^6A-related proteins highlighted in red. (K, bottom panel) Connectivity of m^6A-related proteins compared to other proteins in the network. Statistical significance was calculated using the Wilcoxon test.

Supplemental Figure S2

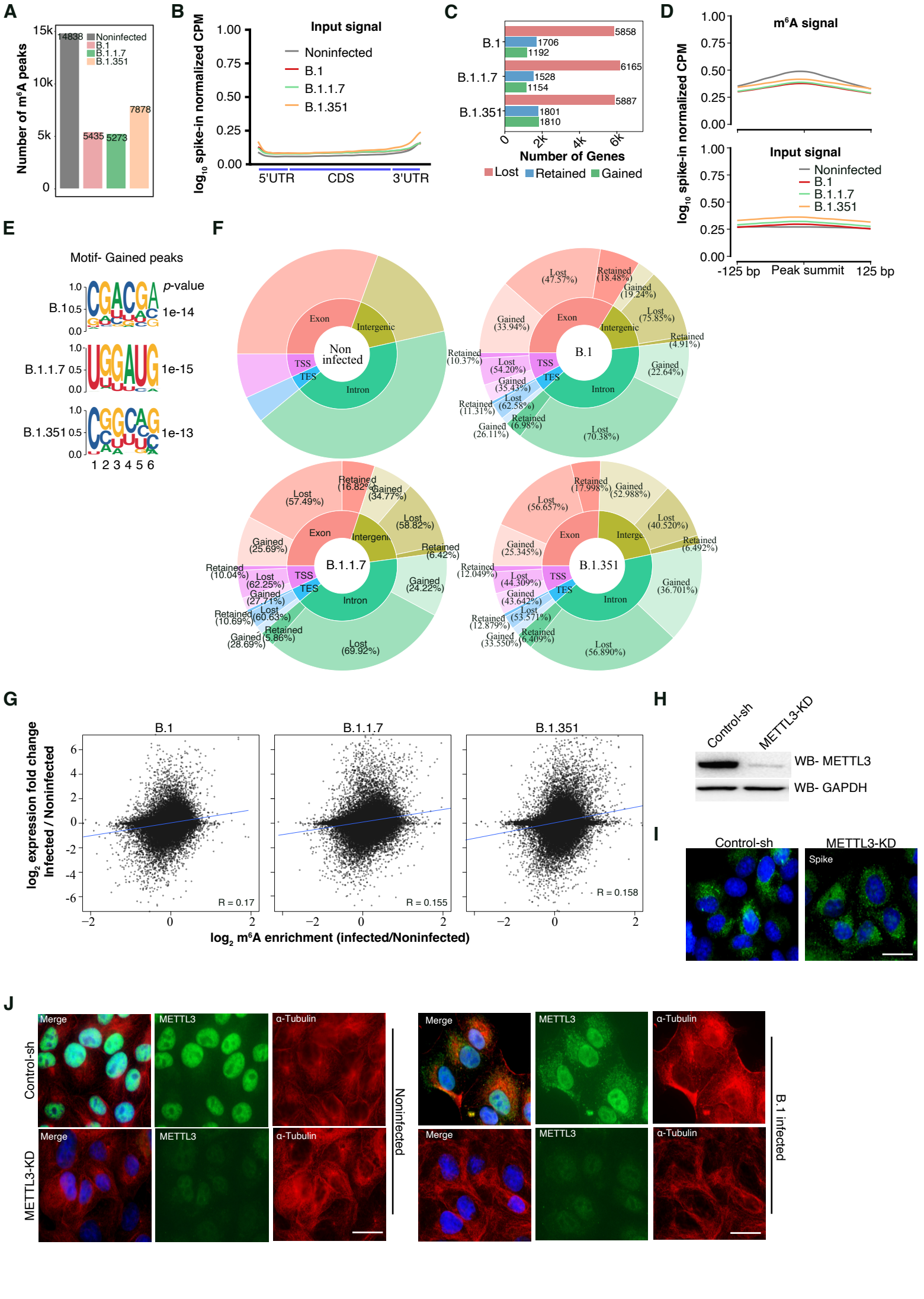

Supplemental Figure S2

K

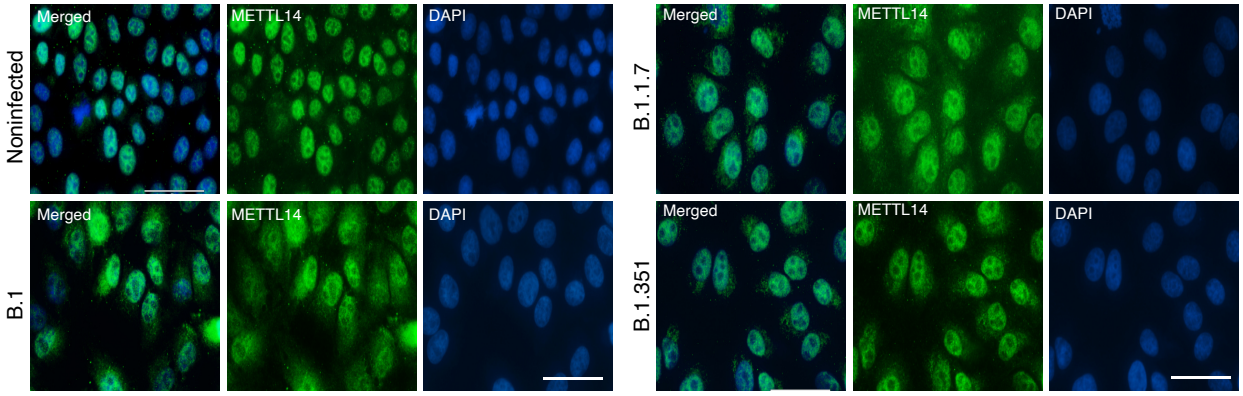

Supplemental_Figure_S2 (A) Number of m^6A peaks in Noninfected and infected Vero cells. (B) Metagene plot showing log_{10} spike-in normalized CPM of Input signals in the saples indiacted. (C) Bar plots representing the number of genes with lost, gained, or retained m^6A peaks in Vero cells after infection with three different SARS-CoV-2 variants, as indicated. (D) log_{10} spike-in normalized CPM of m^6A signal (top panel) and the corresponding input signal (bottom panel) at the m^6A peak regions (± 125bp from m^6A peak summit) that were commonly lost post- infection with the three different variants of SARS-CoV-2 compared to noninfected Vero cells. (E) Identified motifs from *de novo* motif analysis of gained m^6A peaks. Motifs from Vero cells infected with B.1, B.1.1.7, and B.1.351 are shown. (F) Donut plot distribution of annotated m^6A peaks by genomic features for noninfected and infected Vero cells with three different variants, as indicated. The proportion of retained, gained, and lost m^6A peaks annotated in exonic, intronic, transcription start site (TSS), transcription end site (TES), and intergenic regions are shown. (G) Scatter plots depicting the correlation between log_2 fold changes in gene expression and log_2 fold changes in m^6A enrichment after infection with B.1, B.1.1.7, and B.1.351 variants. The blue line depicts linear regression line with 95% confidence interval. Statistics: Pearson's correlation test. (H) Western-blot validation of METTL3 knock-down in Vero cells, with GAPDH used as a loading control. (I) Immunostaining using Spike antibody in control and METTL3-KD cells 48 h post SARS-CoV-2 infection. The scale bar is 20 μm (J) Immunostaining for METTL3 and α-Tubulin in Control and METTL3-KD Vero cells that were either Noninfected or infected with the B.1 SARS-CoV-2 variant. The scale bar is 20 μm (K) Immunostaining showing METTL14 localization in noninfected and Vero cells infected with the B.1, B.1.1.7, B.1.351 variants at 24h. The scale bar is 50 μm.

Supplemental Figure S3

A

Sample	Expected ratio A/m6A	Transition A	Transition m6A	Ratio A/m6A	Average ratio	Avg. number of m6A in 8954 Adenine in viral genome
Standard 1	5	2.26e+05	4.38e+04	5.2		
Standard 2	5	2.30e+05	3.59e+04	6.4	5.4	N/A
Standard 3	5	2.32e+05	4.87e+04	4.8		
SARS-CoV-2 B.1 Exp1	N/A	4.26e+07	6.09e+04	698.7		
SARS-CoV-2 B.1 Exp2	N/A	4.45e+07	4.41e+04	1,008.0	832.0	10.75* +/-1.98
SARS-CoV-2 B.1 Exp3	N/A	3.87e+07	4.89e+04	790.3		

B

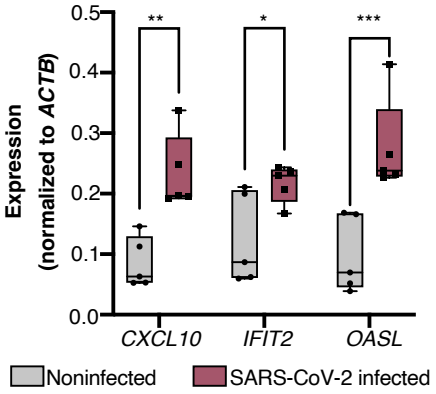

C

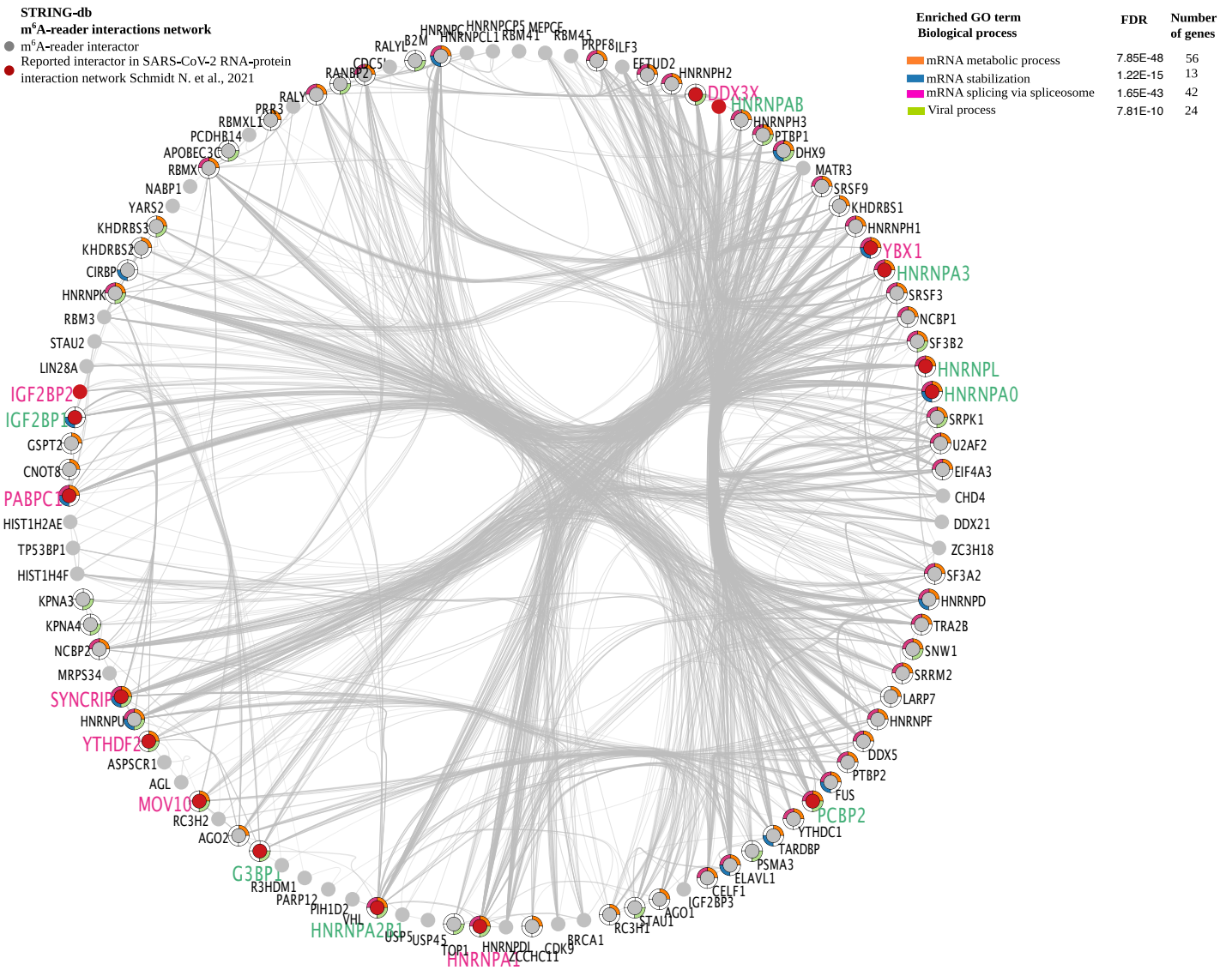

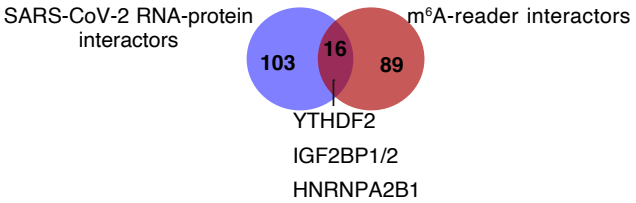

Supplemental_Figure_S3 (A) Summary of LC-MS/MS quantification of m^6A in control standard RNA oligos and B.1 viral genomic RNA. The average ratio of A/ m^6A in the viral genomic RNA was 832. Considering the total number of 'A' in the viral genome to be 8954, the number of 'A' with m^6A modification is on average 10.75 per viral genome. (B) RT-qPCR expression data (normalized to *ACTB*) of three selected genes in RNA isolated from throat/nose swab samples who were either positive (SARS-CoV-2 infected) or negative (noninfected) for COVID-19. (C) Interaction network of m^6A-related proteins. (Top panel) Interaction network of m^6A-related proteins. Known m^6A-reader interacting proteins collected from the STRING- db (grey nodes) were matched with the SARS-CoV-2 RNA-protein interactome obtained from Schmidt et al., 2020 (red nodes). The m^6A-related proteins pertaining to the core or the expanded SARS-CoV-2 interactome (as reported by Schmidt et al., 2021) labeled in pink and green, respectively. Outer node colors indicate enriched GO biological process terms for the m^6A-related proteins of the network. (Bottom panel) The Venn diagram shows the number of overlapping proteins between two datasets as indicated.

Supplemental Figure S4

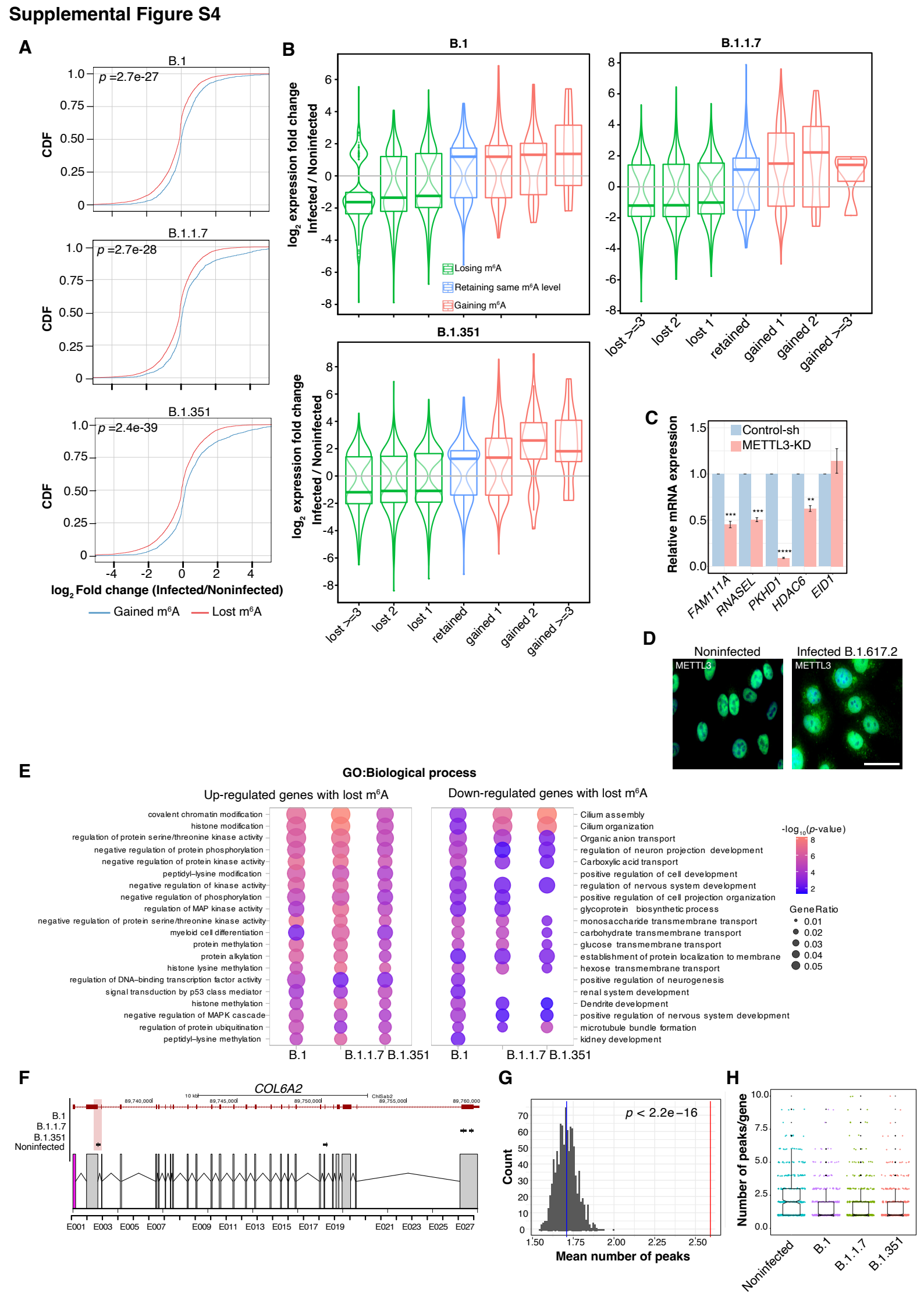

Supplemental_Figure_S4 (A) Cumulative distribution function (CDF) plots showing the cumulative density distribution of $\log_2$ fold changes in gene expression, with a comparison of lost (red) and gained (blue) m^{6}A genes after infection with different SARS-CoV-2 variants. Statistical significance was calculated using the Wilcoxon test. (B) Expression of m^{6}A-modified genes after SARS-CoV-2 infection. The distribution of differentially expressed genes categorized according to changes in m^{6}A levels after viral infection compared to Noninfected cells is shown. Genes were categorized as gaining one or more peaks (non- m^{6}A genes in non-infected cells being m^{6}A -modified after infection), losing one or more peaks (m^{6}A -modified genes in Noninfected cells showing a decrease in m^{6}A peak number), or retaining m^{6}A (showing the same number of m^{6}A peaks in noninfected and infected cells). (C) Relative expression of selected genes with varying levels of m^{6}A modification in METTL3-KD Vero cells compared to control cells. Data was normalized to *GAPDH* expression. Statistics: two- tailed *t*-test; **: $p < 0.01$, ***: $p < 0.001$, ****: $p < 0.0001$, n=3. (D) METTL3 localization in Vero cells infected with the B.1.617.2 (Delta) variant. The scale bar is 50 μm. (E) Top enriched terms associated with up-regulated and down-regulated genes with lost m^{6}A upon infection. The size of the dots depicts the gene enrichment ratio, while their color indicates the $\log_{10}$ level of significance. (F) Differential exon usage for the *COL6A2* gene upon SARS-CoV-2 infection. The genome browser visualization (top) shows the localization of m^{6}A peaks in noninfected and infected cells along the *COL6A2* gene. The exon structure (bottom) with a predicted differentially used exon (DEU) (in pink) included after infection is shown. (G) Distribution of the number of m^{6}A peaks over DEU genes compared to a random distribution in m^{6}A positive genes (1000 replicates without replacement). The average number of m^{6}A peaks in DEU genes and in m^{6}A positive random genes are denoted by a red and blue line, respectively. Statistics: one sample *t*-test. (H) Distribution of m^{6}A peak numbers in DEU genes in noninfected and infected Vero cells (infection with different variants as indicated).

Supplemental Figure S5

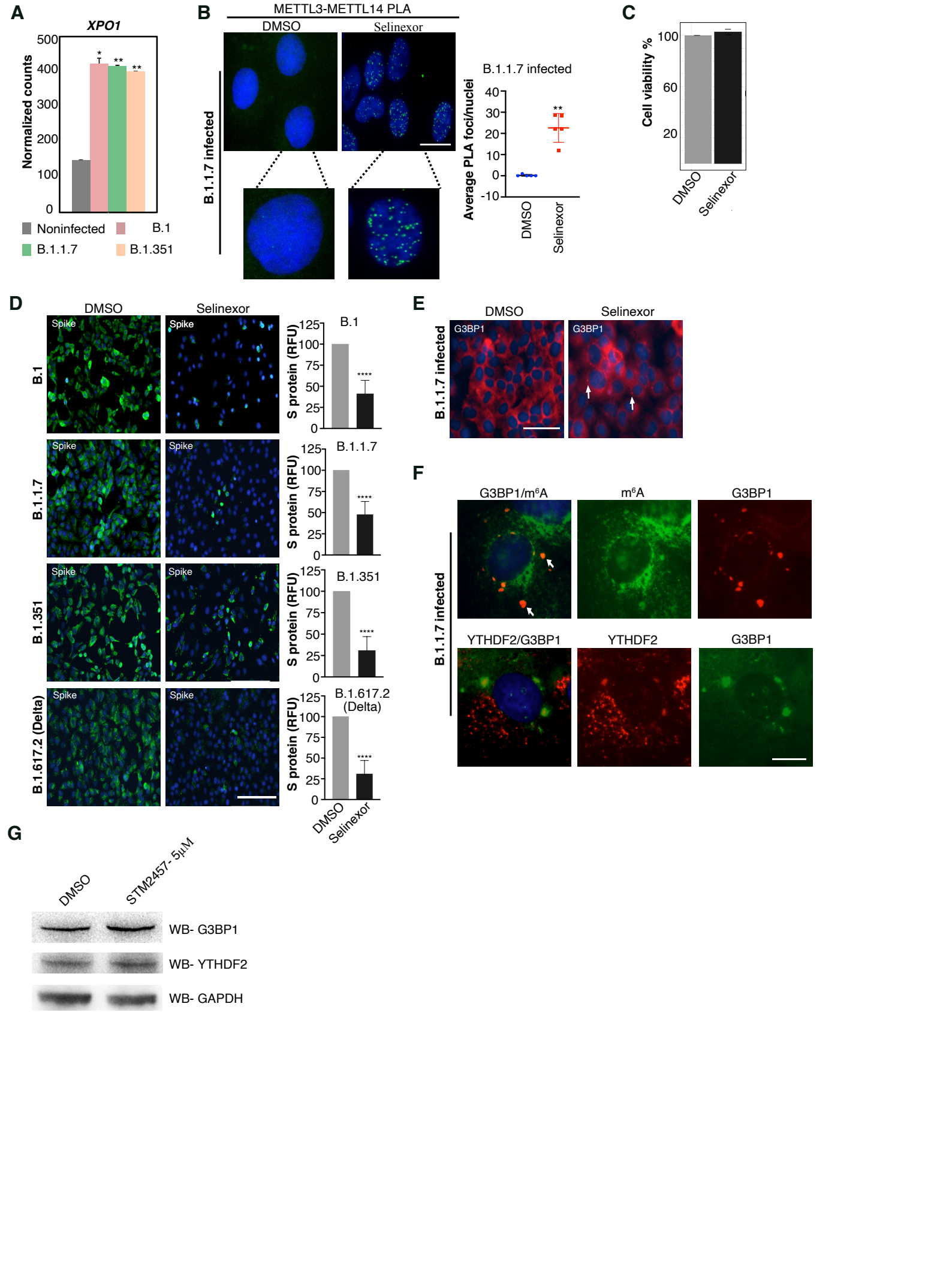

Supplemental_Figure_S5 (A) Bar graph depicting the expression of *XPO1* after infection with the B.1, B.1.1.7, and B.1.351 variants. Normalized read counts in RNA-seq data are reported. (B, left panel) PLA experiment revealing METTL3 and METTL14 interaction foci in the nucleus (marked by DAPI) of Vero cells infected with the B.1.1.7 variant and treated with either DMSO or Selinexor (150nM). The scale bar is 20 μm. (B, right panel) Quantification of METTL3-METTL14 PLA foci as detected in the left panel. The number of PLA foci/nuclei are shown as Mean ± SD. Data presented from multiple experiments with the total number of cells counted ≥100. Statistics: one-way ANOVA, **: $p < 0.01$. (C) MTT assay showing Vero cell viability after Selinexor treatment compared to DMSO control. (D, left) Immunostaining showing SARS-CoV-2 Spike protein in Vero cells at 48 h post-infection with the B.1, B.1.1.7, and B.1.617.2 (Delta) variants, with or without Selinexor treatment. (D, right) Quantification of Spike protein fluorescence in Selinexor-treated and untreated cells infected with different variants, as indicated. Spike fluorescence was quantified in 5 different fields obtained from several experiments. The scale bar is 200 μm. (E) Immunostaining showing G3BP1 localization after Selinexor treatment in B.1.1.7-infected cells at 24 h post-infection. White arrows highlight some of the G3BP1 foci. The scale bar is 50 μm. (F) Immunostaining showing the localization of G3BP1 and m^6A or YTHDF2 after DMSO or Selinexor treatment in B.1.1.7-infected cells at 24 h post-infection. White arrows highlight some of the G3BP1 foci overlapping with the m^6A signal. The scale bar is 10 μm. (G) Western blot detecting G3BP1 and YTHDF2 in Vero cells treated with STM2457 (5 μM) or DMSO. GAPDH was used as a loading control.

Supplemental Figure S6

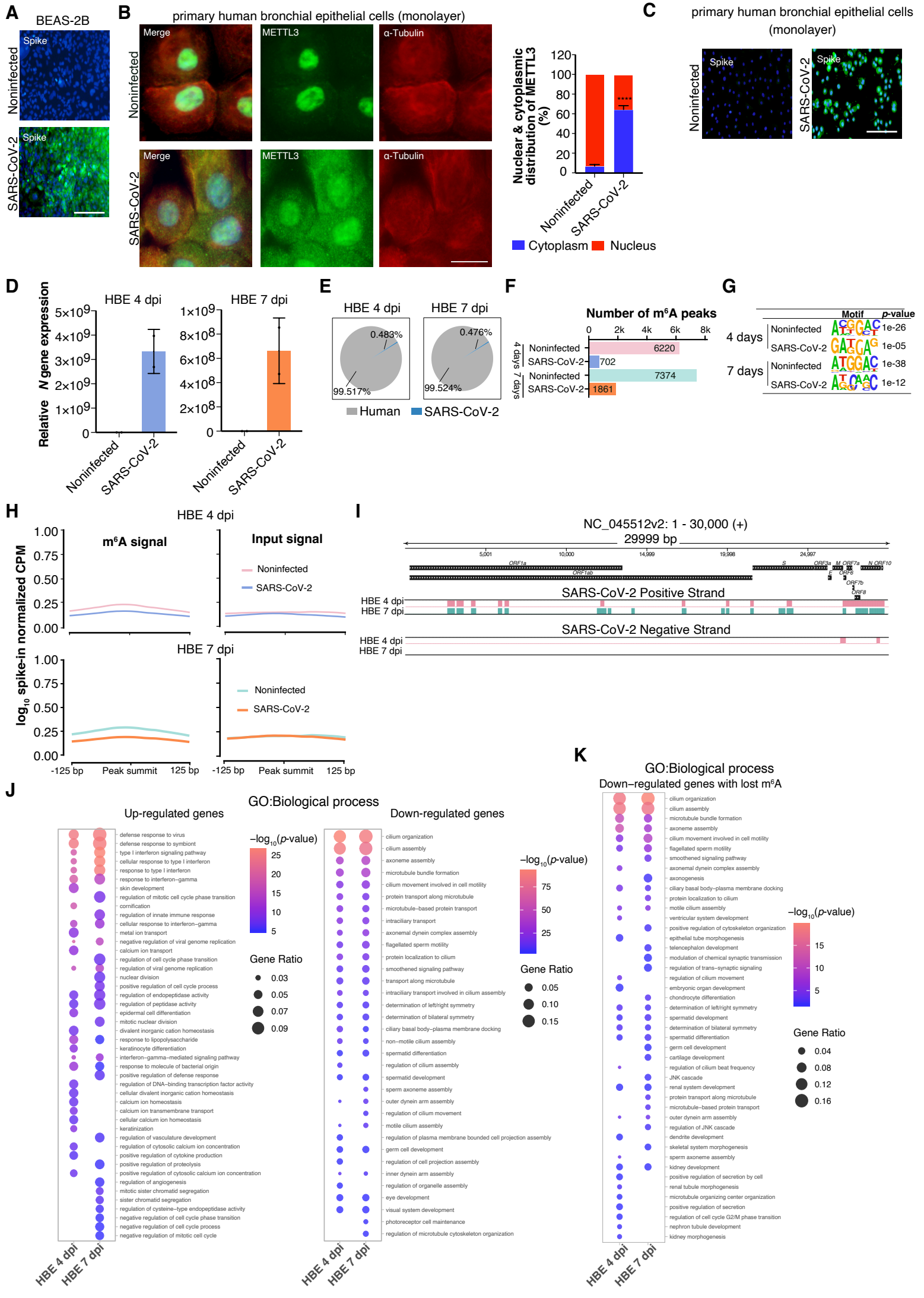

Supplemental_Figure_S6 (A) Spike immunostaining in BEAS-2B cells that were infected with SARS-CoV-2. The scale bar is 200 μm. (B, left panel) METTL3 localization in monolayer culture of Noninfected human primary bronchial epithelial cells and after infection with SARS-CoV-2. The scale bar is 20 μm. (B, right panel) The percentage distribution of METTL3 labeling in the nucleus and cytoplasm was calculated with ImageJ, using DAPI as a nucleus marker and α-Tubulin as a cytoplasm marker. Data are shown as mean ± SD. Data were obtained from multiple experiments with the total number of cells counted ≥110. Statistics: unpaired *t*-test; ****: $p < 0.0001$. (C) Spike protein immunostaining in human primary bronchial epithelial cells grown in monolayer that were infected with SARS-CoV-2. The scale bar is 200 μm. (D) Relative expression of SARS-CoV-2 *N* gene in noninfected and SARS- CoV-2 infected HBE samples 4- and 7- dpi. (E) Pie chart showing the percentage of RNA-seq reads mapping to host (Human) and viral (SARS-CoV-2) genomes in infected HBE samples. (F) Bar plot depicting the number of m^6A peaks in noninfected and SARS-CoV-2 infected HBE at 4- and 7- dpi. (G) Motif analysis of the m^6A peaks in noninfected and infected HBE. (H) $\log_{10}$ spike-in normalized CPM of m^6A signal (left panel) and the corresponding input signal (right panel) at the m^6A peak regions (± 125bp from m^6A peak summit) that were lost in infected HBE at 4- dpi (top) and 7-dpi (bottom) compared to noninfected HBE. (I) Presence of m^6A in the positive and negative strands of the SARS-CoV-2 viral genome at 4- and 7- dpi HBE cells. m^6A peak regions are indicated as colored rectangles. (J) Top GO biological process terms associated with up-regulated and down-regulated genes in HBE at day 4- and 7- dpi with SARS-CoV-2. (K) Top enriched terms associated with lost m^6A genes that were down- regulated in HBE at day 4- and 7- dpi with SARS-CoV-2. (J, K) The size of the dots depicts the gene enrichment ratio, while the color of the dots indicates the $\log_{10}$ level of significance.

Supplemental Figure S7

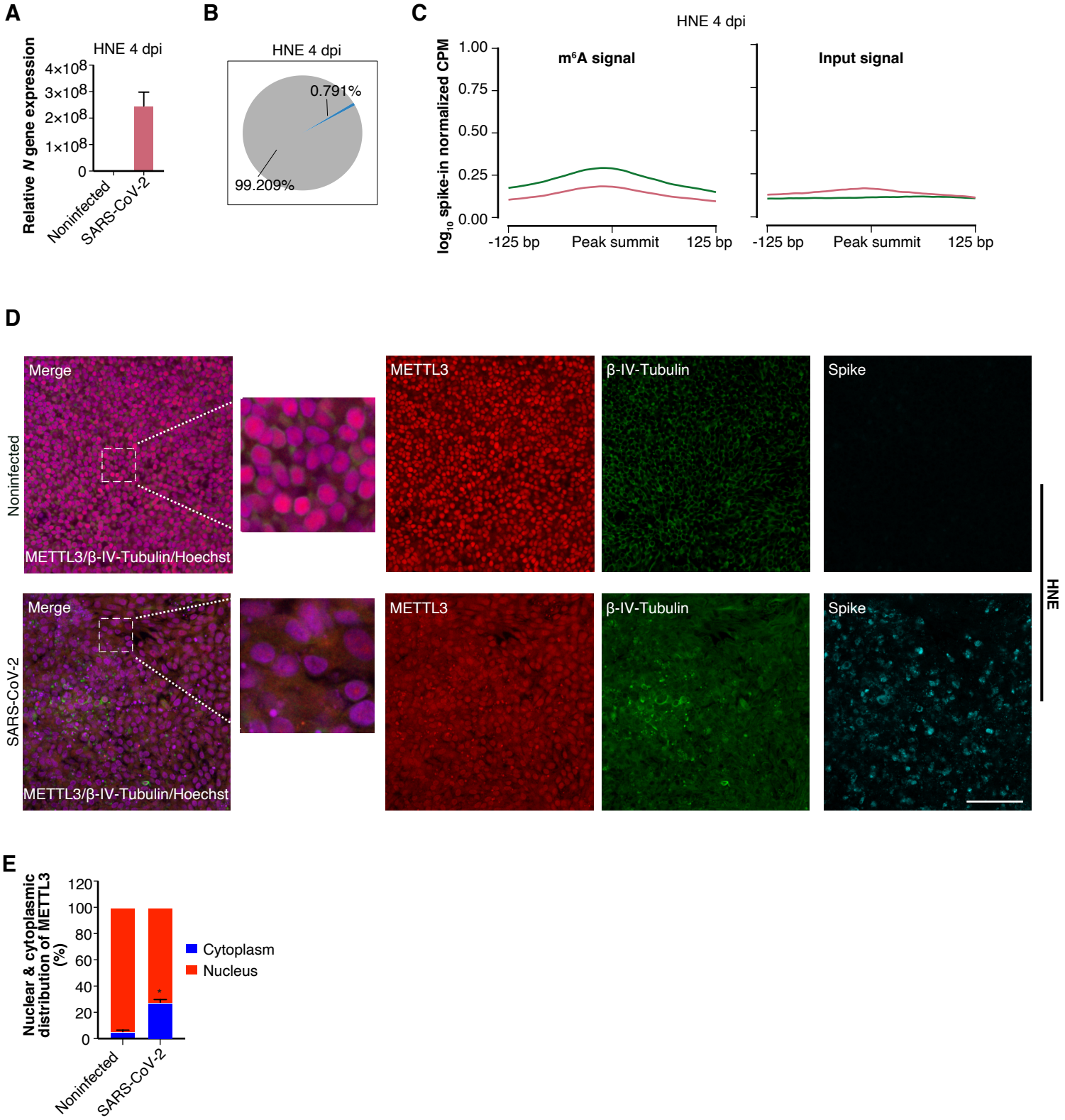

Supplemental_Figure_S7 (A) Relative expression of SARS-CoV-2 *N* gene in noninfected and SARS-CoV-2 infected HNE samples at 4- dpi. (B) Pie chart showing the percentage of reads mapping to the host (Human) and viral (SARS-CoV-2) genomes in infected HNE at 4- dpi. (C) $\log_{10}$ spike-in normalized CPM of m^6A signal (left panel) and the corresponding input signal (right panel) at the m^6A peak regions (± 125bp from m^6A peak summit) that were lost at 4- dpi in infected compared to noninfected HNE. (D) Immunostaining staining showing METTL3 (in red), β-IV-Tubulin (in green) and SARS-CoV-2 spike protein (in cyan) in HNE 4- dpi along with noninfected control. Merged image represents METTL3 and β-IV-Tubulin along with Hoechst. The scale bar is 200 μm. (E) The percentage distribution, of METTL3 in the nucleus and cytoplasm, was calculated using ImageJ. Hoechst was used as a nuclear marker and β-IV-Tubulin marking the cytoplasm. Data are shown as mean ± SD. Data were acquired from n=2 experiments with the total number of cells counted ≥ 1000. Statistics: unpaired t-test; ****: $p < 0.0001$.

Supplemental Tables

Supplemental Table S1: Sequence of oligos used in the study.

Vero		
Primer name	**Sequence**	
FAM111A-Forward primer	CCTTTCCTTCTGGCTCTTCA	
FAM111A-Reverse primer	TGTGGGAGACGGAATAGAGC	
HDAC6-Forward primer	CCCAATCTAGCGGAGGTAAA	
HDAC6-Reverse primer	CGCGATTAGGTCTTCTTCCA	
PKHD1-Forward primer	GTGGGCATTTGGTCTGAAAG	
PKHD1-Reverse primer	AGTTGTCCCAGCAGGACAGT	
RNASEL-Forward primer	TGTCAATGTGAGGGGAGAAA	
RNASEL-Reverse primer	CTTCACCAAACCCAAGTGCT	
EID1-Forward primer	TCGCCTCCTTTTTCACAACT	
EID1-Reverse primer	TGCCATTGAAAAACTTGACCT	
XPO1-Forward primer	TGGTACAGAATGGTCATGGAA	
XPO1-Reverse primer	TCTTCATGCATTGCTCCACT	
YTHDF1-Forward primer	TGGGACAAATGTGAACATGC	
YTHDF1-Reverse primer	TTTAGGCTGTGGTTTTGCAG	
FTO-Forward primer	GGAACCTTATTTTGGCATGG	
FTO-Reverse primer	GCTGACCTGTCCACCAGATT	
SPEN-Forward primer	CCACTCTCTCGGGATCAAAA	
SPEN-Reverse primer	AATCTCGTTTGGAGCGCTAT	
GAPDH-Forward primer	ATGTTCGTCATGGGTGTGAA	
GAPDH-Reverse primer	GGTGCTAAGCAGTTGGTGGT	
POL2RG- Forward primer	ACTGTTGGTGGGTGAGCAC	
POL2RG- Reverse primer	CCAGACTGGCAGCAAGAAAA	
TBP- Forward primer	ACTGTTGGTGGGTGAGCAC	
TBP- Reverse primer	CCAGACTGGCAGCAAGAAAA	
SARS-Cov-2		
Primer name	**Sequence**	
N-protein-Forward primer	CACATTGGCACCCGCAATC	
N-protein-Reverse primer	GAGGAACGAGAAGAGGCTTG	
N-Forward strand	CAGCACTGCTCATGGATTG	Primer for cDNA synthesis
N-Reverse strand	GACCCCAAAATCAGCGAAAT	Primer for cDNA synthesis
Human		
Primer name	**Sequence**	
CXCL10 Forward primer	TGATCTCAACACGTGGACAA	
CXCL10 Reverse primer	ACTGTACGCTGTACCTGCAT	

IFIT2 Forward primer	AAAGGAACCAGAGGCCACTT	
IFIT2 Reverse primer	GCTCGGTTCAGGCAGCTG	
OASL Forward primer	GGACTCTCTGCTCCATCCTC	
OASL Reverse primer	GCAGCCAAGCATCACAAAGA	
ACTB Forward primer	CTCGTAGCTCTTCTCCAGGG	
ACTB Reverse primer	GGGAAATCGTGCGTGACATT	
RNA standard for LC-MS/MS		
RNA oligo with m^6A	GGm^6ACUAAm^6ACU	
RNA oligo without m^6A	GGACUAAACU	
shRNA sequence		
METTL3 shRNA	GCTGCACTTCAGACGAATTAT	
Control shRNA	ATCTCGCTTGGGCGAGAGTAAG	

Supplemental Table S2: Scaling factor used for normalizing m^6A RIP data

Vero	
Sample	**Scaling factor**
Noninfected_m^6A RIP	1
B.1_m^6A RIP	0,72
B.1.7.7_m^6A RIP	0,81
B.1.351_m^6A RIP	0,98
Noninfected_Input	0,76
B.1_Input	0,76
B.1.7.7_Input	0,83
B.1.351_Input	1
HBE	
Sample	**Scaling factor**
HBE Noninfected day 4_m^6A RIP	0,75
HBE SARS-CoV-2 day 4_m^6A RIP	1
HBE Noninfected day 7_m^6A RIP	0,99
HBE SARS-CoV-2 day 7_m^6A RIP	1
HBE Noninfected day 4_Input	1
HBE SARS-CoV-2 day 4_Input	0,92
HBE Noninfected day 7_Input	0,94
HBE SARS-CoV-2 day 7_Input	1
HNE	
Sample	**Scaling factor**
HNE Noninfected_m^6A RIP	0,92
HNE SARS-CoV-2_m^6A RIP	1
HNE Noninfected_Input	0,67
HNE SARS-CoV-2_Input	1

Supplemental methods

Cell culture, SARS-CoV-2 infection and XPO1 inhibitor treatment

B.1 is the lineage with the D614G spike amino acid change. B.1.1.7 is the Alpha variant (WHO label) and the earliest documented variant in the UK (Sep-2020). B.1.1.351 is the Beta variant (WHO label) and was first documented in South Africa (May 2020). T25 flasks with Vero CCL-81 (ATCC) were infected with the three different SARS-CoV-2 variants (1000 $TCID_{50}$) and medium or infected cells were harvested in TRIzol 48 h post-infection for RNA-sequencing studies. In all cases, the amount of infection was verified by immunostaining and RT-qPCR (see method below). Vero CCL-81 cells were cultured in chamber slides and the different SARS-CoV-2 variants were diluted in medium to 1000 $TCID_{50}$ (DMEM with 1% penicillin-streptomycin and 2% fetal calf serum), supplemented with DMSO or Selinexor (150nM). 200 µl of the diluted virus was added to each well and the slides were incubated for 24 h at 37°C at 5% CO_2. The cells were fixed using 4% formaldehyde in PBS for 10 min at room temperature (RT) in chamber slides and washed three times in PBS.

Primary human bronchial epithelial cells (Lonza, CC-2540S) and bronchial epithelial cell line BEAS-2B (ATCC) were received as a gift from Professor Madeleine Rådinger group, Gothenburg University, Sweden, and were cultured in monolayer following manufacturer instructions. Primary human bronchial epithelial and BEAS-2B cells were infected with the B.1.1.7 variant of SARS-CoV-2 in a similar way to Vero cells as described above in their corresponding culture media and fixed using 4% formaldehyde in PBS for 10 min at RT in chamber slides 72 h post-infection.

SARS-CoV-2 infection of reconstructed human bronchial and nasal epithelia

MucilAir™ cultures, corresponding to reconstructed human bronchial and nasal epithelia (HBE and HNE, respectively) differentiated at the air/liquid interface (ALI), were purchased from Epithelix (Saint-Julien-en-Genevois, France). Cultures were maintained in ALI conditions in transwells with 700 µL of MucilAir™ medium (Epithelix) in the basal compartment and kept at 37°C under a 5% CO_2 atmosphere. SARS-CoV-2 infection was performed in epithelial cultures as previously described (Robinot et al. 2021). Briefly, the apical side of ALI cultures was washed once, and cells were then incubated with the isolate BetaCoV/France/IDF00372/2020 (EVAg collection, Ref-SKU: 014V-03890)

diluted in 150 µl of DMEM medium. The viral input was left on the apical side for 4 h at 37 °C, and then removed by 3 apical washes. Positivity for SARS-CoV-2 infection was tested by RT-qPCR as described below.

Immunofluorescence Staining

Cells were fixed with 4% formaldehyde for 10 min, followed by two washes with phosphate-buffered saline (PBS). Then cells were permeabilized using 0.25% Triton X-100 in PBS for 10 min followed by two washes with PBS-0.1% Tween 20 (PBST). Blocking was performed in 3% bovine serum albumin (BSA) in PBST for an hour at RT. The cells were incubated overnight at 4 °C with the following primary antibodies: anti-METTL3 rabbit antibody (1:300, ab195352; Abcam), anti-METTL14 rabbit antibody (1:300, HPA038002; Atlas Antibodies), anti-α-Tubulin mouse antibody (1:1000, T5168; Merck), anti-SARS-CoV-2 Spike glycoprotein rabbit antibody (1:300, ab272504; Abcam), anti-G3BP mouse antibody (1:500, ab56574; Abcam), anti-m^6A rabbit antibody (1:400, 202003, Synaptic Systems), and anti-YTHDF2 rabbit antibody (1:100, ab246514; Abcam). The slides were washed three times for 5 min in PBST and subsequently incubated with secondary antibodies conjugated with Alexa Fluor 488 and Alexa Fluor 555 fluorochromes (1:800; Invitrogen), for an hour in the dark at RT. After incubation with the secondary antibodies, cells were washed three times for 5 min in PBST. Prolong Gold with DAPI (Thermo Fisher Scientific–Life Technologies) was added to each coverslip and air-dried in the dark to detect nuclei. Slides were imaged in a fluorescence microscope (EVOS™ FL Auto, Thermo Fisher Scientific) using 20X and 60X oil immersion objectives by keeping the same parameter during image acquisition.

For immunofluorescence staining in HNE, MucilAir^{TM} cultures were fixed in 4% PFA for 30 mins at RT, washed two times with PBS, and cut using a scalpel blade. Membrane pieces were placed in 10 µl drops on parafilm, and subsequent staining steps were performed on parafilm at RT. Cells were permeabilized with 0.5% Triton X-100 in PBS for 20 min and then blocked in 0.1% Tween 20, 1% bovine serum albumin (BSA), 10% fetal bovine serum, 0.3 M glycine in PBS for 30 min. Samples were incubated overnight at 4°C with AF647 conjugated rabbit anti-METTL3 primary antibody (ab217109; Abcam; 1:100 dilution), AF488 conjugated rabbit anti-β-IV-Tubulin (ab204003; Abcam; 1:250 dilution) and anti-spike (1:100, is a gift from Hugo Mouquet (Pasteur Institute). The samples were

washed thrice in PBS followed by one hour incubated at RT with secondary antibody AF555-conjugated goat anti-mouse (1:500 dilution). Samples were counterstained with Hoechst and mounted in FluoromountG (Thermo Fisher Scientific) before observation with a Leica TCS SP8 confocal microscope (Leica Microsystems).

For quantification of METTL3 localization, images were analyzed with ImageJ. Fluorescence channels corresponding to the nuclear marker (DAPI/ Hoechst) and cytoplasmic marker (anti- α-Tubulin or anti-β-IV-Tubulin) were split to mark the nuclear and cytoplasmic border followed by quantification of METTL3 intensity (Relative Fluorescence Unit: RFU) in nucleus and cytoplasm.

RT-qPCR and m^{6}A RIP-qPCR

For performing m^{6}A RIP-qPCR, 3 µg of RNA from Vero cells infected with SARS-CoV-2 B.1.1.7 variant or human patient RNA samples from throat/nose swabs (ethical permit # 2020-03276, #2020-01945 and #2022-01139-02) were used. RIP was performed with 1µg of m^{6}A antibodies (synaptic systems, 202003) or IgG antibodies (SantaCruz, SC-2027). The input and m^{6}A RIP-RNA were converted to cDNA using the High-Capacity RNA-to-cDNA™ Kit (Thermo Fisher Scientific, 4387406) and random primers. qPCR was performed on a Quant Studio 3 thermocycler (Thermo Fisher Scientific) using gene-specific PCR primers (**Supplemental Table S1**) mixed with Power SYBR Green Master Mix (Thermo Fisher Scientific, 4367659) and diluted cDNA (10-fold dilution) as a template. The data is represented as percentage input values.

For RT-qPCR, the RNA was directly converted to cDNA and subjected to qPCR as mentioned above, using primers listed in Supplemental Table S1. Expression values presented for each gene are normalized to *TBP* and *POL2RG* or to *GAPDH* using the delta-delta Ct method.

To check m^{6}A levels in both forward and reverse strands of the viral RNA, cDNA was synthesized with primers specific for each strand separately at 50 °C (**Supplemental Table S1**) using the ImProm-II™ Reverse Transcription System (Promega, A3800) and subjected to qPCR with primers specific for the viral N-protein (**Supplemental Table S1**).

Human patient RNA samples from throat/nose swabs were converted to cDNA and subjected to qPCR as mentioned above, using primers listed in Supplemental Table S1. Expression was normalized to *ACTB*.

The cellular level of SARS-CoV-2 RNA was measured by RT-qPCR in HBE and HNE infection as described previously (Samelson et al. 2022).

G3BP1 and YTHDF2 RNA Immuno-precipitation qPCR (RIP-qPCR)

Uninfected Vero cells treated with the METTL3 inhibitor STM2457 (5μM for 48h) or with DMSO were harvested and fixed for 10 mins with formaldehyde (1% final concentration) and quenched with Glycine (0.125 M, final concentration). Fixed cells were lysed in RIPA buffer (50mM Tris pH7.4, 150mM NaCl, 0.5% Sodium Deoxycholate, 0.2% SDS, 1% IGEPAL-CA630, Protease inhibitor, and RNase inhibitor) and sonicated for 10 cycles (30 secs on 30 secs off) on a Bioruptor (Diagenode) sonicator. The cleared lysate was used for RIP with anti-G3BP1 (Abcam, Ab181150), anti-YTHDF2 (Abcam, Ab246514) and IgG (SantaCruz, SC-2027) antibodies. The RNA-protein-antibody complex was captured using protein A/G magnetic beads (Thermo Fisher Scientific, 10002D and 10004D). Magnetic beads were washed with low salt buffer (1X PBS, 0.1% SDS and 0.5% IGEPAL-CA630) and high salt buffer (5X PBS, 0.1% SDS and 0.5% IGEPAL-CA630) before eluting in elution buffer (10mM Tris pH7.4, 100mM NaCl, 1mM EDTA, 0.5% SDS) with Proteinase K. RNA was extracted using TRIzol reagent and cDNA synthesis and RT-qPCR were performed as described above. The data is represented as percentage input values.

LC-MS/MS quantification of m^6A in viral RNA

LC-MS/MS-based quantification of m^6A was done as previously described (Liu et al. 2021, 2020a). In brief, RNA from B.1 viral particles was isolated from Vero cell supernatant and digested by P1 nuclease (Sigma, N8630) followed by treatment with phosphatase (NEB, M0289S). The sample was then filtered (0.22 μm pore size) and directly injected into the LC-MS apparatus. As a positive standard for LC-MS/MS, and to estimate the number of m^6A modifications in viral RNA, we parallelly processed commercially synthesized RNA oligos (**Supplemental Table S1**) with or without internal m^6A mixed at a 5:1 A/m^6A ratio. We made triplicate injections of the standard RNA oligos and the viral RNA and estimated the A/m^6A ratios for both samples. LC-MS/MS profiles were monitored using the parallel reaction-monitoring (PRM) mode for: m/z 268.0–136.0, and m/z 282.0–150.1 that corresponds to A and m^6A respectively, as previously described (Sun et al. 2021).

METTL3 knock-down and Western blot analysis

Vero cells with stable METTL3 (METTL3-KD) and control knockdown (Control-sh) were generated using lentivirus expressing shRNA against METTL3 or non-targeting genomic regions. The shRNA sequences used in the study are provided in Supplemental Table S1.

Total proteins were extracted from cells using RIPA buffer (Sigma-Aldrich, #R0278) and quantified using the Pierce BCA Protein Assay Kit (Thermo Scientific, #23225) as per the manufacturer's instructions. An equal amount of proteins per sample were resolved by SDS- PAGE on NuPAGE Bis-Tris gels (4-12%) (Invitrogen), followed by transfer onto 0.2 μm Nitrocellulose membrane using a Trans-Blot Turbo Transfer System (Bio-Rad). The membrane was blocked for 1 h at RT with a blocking solution (PBST- 5%Milk) before incubation with the primary antibodies, anti-METTL3 (1:400, Ab195352; Abcam), anti-G3BP1 (1:1000, Abcam, Ab181150), anti-YTHDF2 (1:1000, Abcam, Ab246514) or anti-GAPDH (1:5000, ab9485, Abcam), in blocking solution overnight at 4°C. After washing, the membranes were incubated with a secondary antibody for 1 h at RT, and the proteins were then detected with the SuperSignal West Pico PLUS Chemiluminescent Substrate (Thermo Scientific, #34579) using a ChemiDoc XRS+ system (Bio-Rad).

Proliferation assay

5,000 cells/well were seeded in a 96-well plate to assess the proliferation of cells treated with either DMSO or Selinexor (150nM). The CellTiter 96 Non-Radioactive Cell Proliferation Assay kit (Promega, #G4000) was used to determine cell growth as per the manufacturer's instructions. Absorbance was measured using a microplate reader Infinite 50 (Tecan, Austria).

Excluding potential N6,2′-*O*-dimethyladenosine (m^6Am) signals

To evaluate the presence of potential m^6Am modification located at the first-transcribed nucleotide (Tan et al. 2018; Liu et al. 2020b), we bioinformatically excluded m^6A RIP-seq signals located near the transcription start sites (TSS) that could correspond to m^6Am modifications captured by the m^6A antibody. For this, the summit coordinates of predicted m^6A RIP-seq peaks were overlapped with the first 20 nt (close to transcription start sites) of all transcripts using the plyranges package (Lee et al. 2019) according to each reference genome (chlsab2, hg38 or wuhCor1). The m^6A peaks located within the 20 bp regions from transcription start sites were excluded from the analysis.

Quantification of viral reads

Counts of reads uniquely mapped to the SARS-CoV-2 genome were obtained with featureCounts (Liao et al. 2019) and normalized to the spike-in scaling factor. TPM values were then calculated using these counts by further normalizing with the gene lengths to obtain viral gene expression. Averaged TPM expression values were calculated for all replicates in Vero, HBE, and HNE post-infection samples, reflecting the different numbers of viral reads depending on the host cells.

Analysis of m^{6}A-readers from publicly available SARS-CoV-2 interactome

We collected publicly available data from the SARS-CoV-2 interactome in Schmidt et al., 2021 to analyze the reported interactions of known m^{6}A-readers. For this, we selected proteins with a significant $\log_2$ enrichment over the background. As reported by the original authors, the SARS-CoV-2 RNA-protein interactome can be further divided into a core (adjusted p-value < 0.05) and expanded interactome (adjusted p-value < 0.2), containing 57 and 119 RNA interacting proteins, respectively. After matching the significantly enriched SARS-CoV-2 RNA-protein interactome data with the publicly available m^{6}A-reader protein interactors collected from STRINGdb, we found 16 overlapping proteins. From these, 8 proteins belong to the core SARS-CoV-2 RNA-protein interactome (YTHDF2, YBX1, SYNCRIP, PABPC1, MOV10, DDX3X, HNRNPA1, and IGF2BP2) and 8 proteins (IGF2BP1, HNRNPA3, HNRNPA0, HNRNPAB, HNRNPL, G3BP1, PCBP2, and HNRNPA2B1) form part of the expanded SARS-CoV-2 interactome. The resulting interaction network was analyzed and visualized using StringApp Cytoscape plugin (Doncheva et al. 2019).

Analysis of RNA-seq data for differential gene expression

Aligned reads were quantified using featureCounts from the Rsubread package (Liao et al. 2019) following differential expression analysis with DESeq2 using two replicates per condition (Love et al. 2014). Genes were considered differentially expressed if they had an absolute $\log_2$ fold change value > 1 and an adjusted p-value cutoff of < 0.01 for Vero data and $\log_2$ fold change > 0.5 and adjusted p-value < 0.1 for HBE data. Heatmap visualization of differentially expressed genes was generated using the pheatmap package in R. Principal component analysis of gene expression patterns after infection with different SARS-CoV-2 variants was calculated on the regularized normalized counts obtained from DESeq2 using the factoextra package. Correlation analysis of the gene expression changes was

performed between cells infected with different SARS-CoV-2 variants and also at the level of differentially expressed genes in different infection conditions. Publicly available data were used as well (Riva et al. 2020). Functional enrichment analysis was carried out using clusterProfiler (Yu et al. 2012) or Enrichr (Chen et al. 2013) against the Gene Ontology biological process or Enrichr COVID-19 related gene sets databases, respectively, with the selection of significantly enriched terms (*p*-value < 0.05). GO term clustering and visualization analysis was carried out using ClueGO (Bindea et al. 2013) from Cytoscape v3.8.2. Briefly, common enriched terms across any pair of variants previously identified with clusterProfiler and associated with m^6A related genes were selected and their relationships were analyzed using ClueGO, enabling the visualization of shared genes between common terms. Calculation of network connectivity and comparison to random networks were performed using the igraph R package (https://cran.r-project.org/package=igraph). Differential exon usage analysis was performed with the DEXSeq R/Bioconductor package (Anders et al. 2012) on TPM normalized sequence counts quantified with Salmon v1.4.0 (Patro et al. 2017) in mapping-based mode using the stranded reverse library type parameter (-l SR).

Reference:

Anders S, Reyes A, Huber W. 2012. Detecting differential usage of exons from RNA-seq data. *Genome Res* **22**: 2008–17.

Bindea G, Galon J, Mlecnik B. 2013. CluePedia Cytoscape plugin: pathway insights using integrated experimental and in silico data. *Bioinformatics* **29**: 661–3.

Chen EY, Tan CM, Kou Y, Duan Q, Wang Z, Meirelles GV, Clark NR, Ma'ayan A. 2013. Enrichr: interactive and collaborative HTML5 gene list enrichment analysis tool. *BMC Bioinformatics* **14**: 128.

Doncheva NT, Morris JH, Gorodkin J, Jensen LJ. 2019. Cytoscape StringApp: Network Analysis and Visualization of Proteomics Data. *J Proteome Res* **18**: 623–632.

Lee S, Cook D, Lawrence M. 2019. plyranges: a grammar of genomic data transformation. *Genome Biol* **20**: 4.

Liao Y, Smyth GK, Shi W. 2019. The R package Rsubread is easier, faster, cheaper and better for alignment and quantification of RNA sequencing reads. *Nucleic Acids Res* **47**: e47.

Liu J, Dou X, Chen C, Chen Chuan and Liu C, Xu MM, Zhao S, Shen Bin and Gao Y, Han D, He C. 2020a. N 6-methyladenosine of chromosome-associated regulatory RNA regulates chromatin state and transcription. *Science (1979)* **367**: 580–586.

Liu J, Li K, Cai J, Zhang M, Zhang X, Xiong X, Meng H, Xu Xizhan and Huang Z, Peng J, Fan J, et al. 2020b. Landscape and Regulation of m6A and m6Am Methylome across Human and Mouse Tissues. *Mol Cell* **77**: 426–440.e6.

Liu J, Xu Y-P, Li K, Ye Q, Zhou H-Y, Sun H, Li X, Yu L, Deng Y-Q, Li R-T, et al. 2021. The m6A methylome of SARS-CoV-2 in host cells. *Cell Res* **31**: 404–414.

Love MI, Huber W, Anders S. 2014. Moderated estimation of fold change and dispersion for RNA-seq data with DESeq2. *Genome Biol* **15**: 550. http://www. (Accessed December 28, 2022).

Patro R, Duggal G, Love MI, Irizarry RA, Kingsford C. 2017. Salmon provides fast and bias-aware quantification of transcript expression. *Nat Methods* **14**: 417–419.

Riva L, Yuan S, Yin X, Martin-Sancho L, Matsunaga N, Pache L, Burgstaller-Muehlbacher S, de Jesus PD, Teriete P, Hull M v, et al. 2020. Discovery of SARS-CoV-2 antiviral drugs through large-scale compound repurposing. *Nature* **586**: 113–119.

Robinot R, Hubert M, de Melo Guilherme Dias and Lazarini F, Bruel T, Smith N, Levallois S, Larrous F, Fernandes J, Gellenoncourt S, Rigaud S, et al. 2021. SARS-CoV-2 infection induces the dedifferentiation of multiciliated cells and impairs mucociliary clearance. *Nat Commun* **12**: 4354.

Samelson AJ, Tran QD, Robinot R, Carrau L, Rezelj V v, Kain A mac, Chen M, Ramadoss GN, Guo X, Lim SA, et al. 2022. BRD2 inhibition blocks SARS-CoV-2 infection by reducing transcription of the host cell receptor ACE2. *Nat Cell Biol* **24**: 24–34.

Schmidt N, Lareau CA, Keshishian H, Ganskih S, Schneider C, Hennig T, Melanson R, Werner S, Wei Y, Zimmer M, et al. 2021. The SARS-CoV-2 RNA-protein interactome in infected human cells. *Nat Microbiol* **6**: 339–353.

Sun H, Li K, Zhang X, Liu J, Zhang M, Meng H, Yi C. 2021. m6Am-seq reveals the dynamic m6Am methylation in the human transcriptome. *Nat Commun* **12**: 4778.

Tan B, Liu H, Zhang S, da Silva SR, Zhang L, Meng J, Cui X, Yuan H, Sorel O, Zhang S-W, et al. 2018. Viral and cellular N6-methyladenosine and N6,2'-O-dimethyladenosine epitranscriptomes in the KSHV life cycle. *Nat Microbiol* **3**: 108–120.

Yu G, Wang L-G, Han Y, He Q-Y. 2012. clusterProfiler: an R package for comparing biological themes among gene clusters. *OMICS* **16**: 284–7.